MNRAS **000**, 1–3 (2015) Preprint 9 February 2023 Compiled using MNRAS LATEX style file v3.0

Multiband study of Mrk 231

Ailing Wang,[1,2]

[1]*Shanghai Astronomical Observatory, Key Laboratory of Radio Astronomy, CAS, 80 Nandan Road, Shanghai 200030, China*
[2]*University of Chinese Academy of Sciences, 19A Yuquanlu, Beijing 100049, China*

Accepted XXX. Received YYY; in original form ZZZ

ABSTRACT

Mrk 231, also known as UGC 08058 and IRAS 12540+5708 at a redshift $z = 0.042$, is one of the local Universe's most luminous infrared galaxies and the closest known radio-quiet quasar. Mrk 231 has emerged as the standard for quasar-driven winds at the galactic scale. It is an ideal laboratory for studying active galactic nucleus (AGN) feedback because it has powerful multi-phase, multi-scale outflows and a radio jet. Here, we will introduce shortly multi-band study of Mrk 213 but more emphasis on radio data study.

Key words: galaxies: ISM – galaxies: jets – galaxies: kinematics and dynamics – quasars:absorption lines – quasars: individual (Mrk 231)

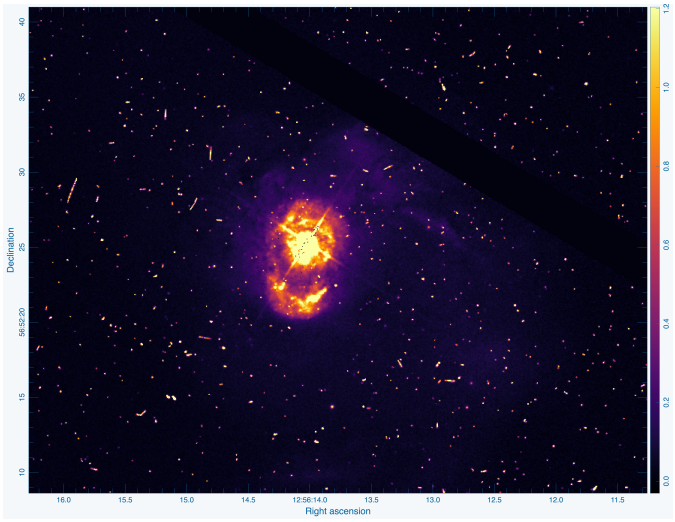

Figure 1. Hubble space telescope (HST) image of Mrk 231.

1 OPTICAL AND INFRARED DATA

1.1 continuum spectrum

Mrk 231 was identified as a SA galaxy according to optical morphology (see Fig. 1). The optical morphology clearly demonstrates that Mrk 231 is an ongoing major merger (e.g., Veilleux et al. 2002, 2006). Mrk 231 hosts an AGN and a young, dusty starburst characterised by a star formation rate (SFR) of $\sim 160 M_{\odot}$ yr^{-1} (Veilleux et al. 2009).

1.2 far-ultraviolet (FUV) spectrum

In this section, we will show a far-ultraviolet (FUV) spectrum of this object covering ∼1150-1470 Åwith the Cosmic Origins Spectrograph on board the Hubble space telescope (HST). Fig. 2 is dominated by broad, highly blueshifted Lyα emission, it does also present a number of faint but significant "bumps" and "wiggles". The object should have strong broad absorption in Lyα possibly also emission and absorption from 1118-1403 Å. Mrk231's broad Lyα emission has a blueshift of 3500 km s^{-1}, which is unusual for AGNs. The median blueshift of Lyα in low-redshift unobscured quasar is of ~ -400 km s^{-1} (Kramer & Haiman 2009). Surprisingly, there are no clear broad absorption features in the FUV spectrum either. As a result, it doesn't appear to be filtered by the dusty iron low-ionization broad absorption line (FeLoBAL) screen and appears to be dominated by AGN rather than star formation. The FUV continuum emission is probably produced by the AGN accretion disk and the outflowing BLA cloud system generates the Lyα emission (Veilleux et al. 2013).

1.3 Chemical component from outflow

In the A-array 3 mm data (see Fig. 3 - top panel), there are spectral lines of HCN, HCO$^+$, SiO, CCH, H^{1}3CN, HC^{1}5N, and H^{1}3CO$^+$. In the A-array 2 mm data (see Fig. 3 - bottom panel), there are spectral lines of HCN, HCO$^+$ 1-0 and 2-1 lines show very wide line wings with a full width at zero intensity of 1500–2000 km s^{-1}. Mrk 231 has a larger HCN line core emission than HCO$^+$ and HNC line core emissions. Although optical-depth broadening of the HCN line is more likely the cause, this could be HCN emission occurring at forbidden velocities. The varying velocities of the HCN, HCO$^+$, and HNC emission line wings all point to a clumpy, chemically

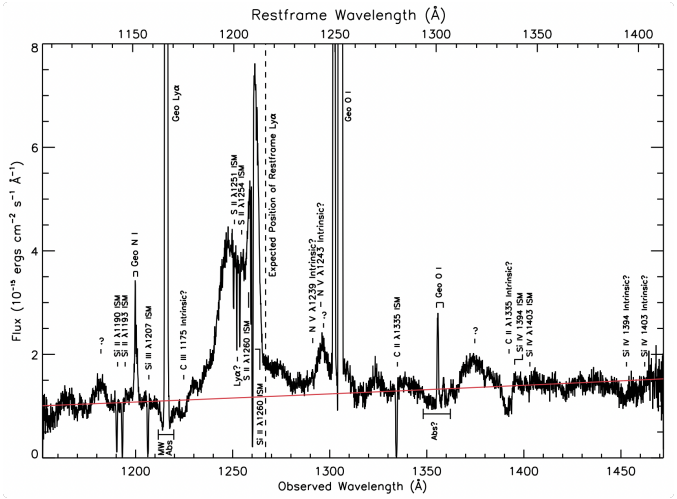

Figure 2. HST-COS FUV spectrum of Mrk 231, binned by ten spectral pixels to highlight the fainter details (Veilleux et al. 2013).

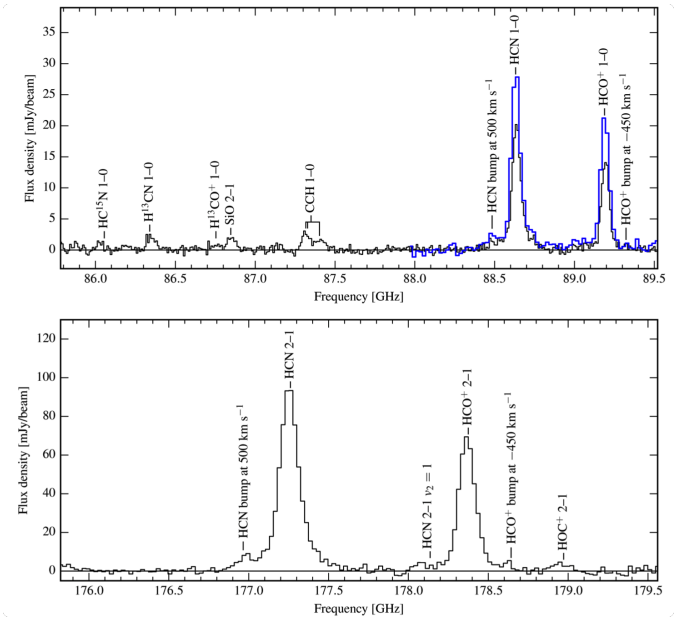

Figure 3. Top: 3 mm A-array (black line) and B–array (thick blue line; Aalto et al. (2012)) spectra of Mrk 231 towards the central beam. Bottom:2 mm D–array spectrum (Lindberg et al. 2016).

distinct outflow. We demonstrate through the use of radiative transfer modeling that, despite the fact that the HCN emission is in line with a clumpy outflow, when the same model properties are applied to the HCO^+ emission, they result in unrealistically high outflow masses that are also in line with the HCN modelling results. This suggests that structures with distinct physical properties are the source of the HCN and HCO^+ emissions (Lindberg et al. 2016).

2 X-RAY DATA

The source was found, albeit at much fainter levels than previously thought. This was probably caused by contamination in the large

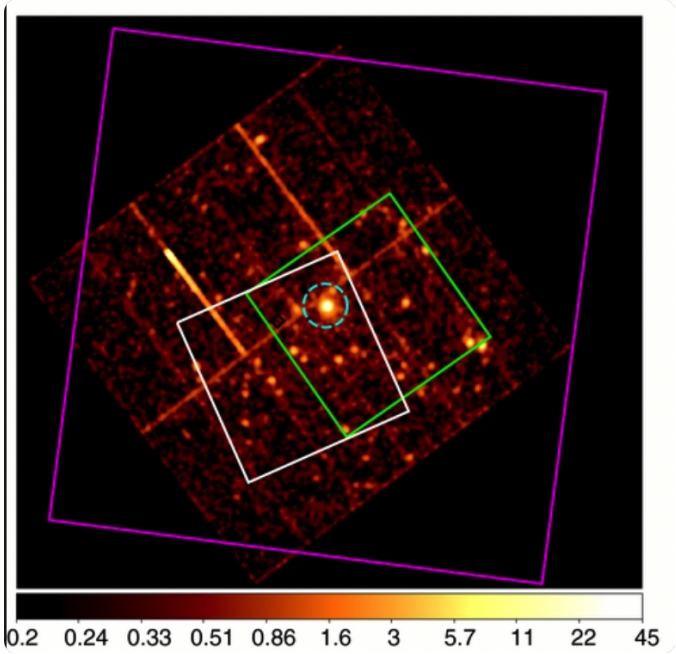

Figure 4. An image of the Mrk 231 field taken by EPIC-pn of the XMM-Newton Telescope in the range of 0.5–10 keV (ObsID: 0081340201). The data, which were smoothed with a Gaussian with a radius of four pixels and minimally processed, clearly demonstrate the richness of the field surrounding Mrk 231. The dashed cyan circle denotes the Mrk 231 spectral extraction region in the NuSTAR FOV of the first (white) and second (green) epochs. Additionally, the Suzaku PIN HPD (34' by 34') is depicted in magenta. In terms of counts per pixel, the color bar represents log intensity.

apertures of previous hard X-ray telescopes that did not focus. The active galactic nucleus (AGN) in Mrk 231 is suggested by the full band X-ray spectrum (0.5–30 keV). It is a nearby illustration of a low-ionization expansive ingestion line quasar that is inherently X-beam powerless. The feeble ionizing continuum might make sense of the absence of mid-infrared [O_{IV}], [Ne_V], and [Ne_{IV}] fine-structure emanation lines which are available in sources with in any case comparable AGN properties. We contend that the characteristic X-beam shortcoming might be a consequence of the super-Eddington growth happening in the core of this ULIRG, and may likewise be normally connected with the strong breeze occasion seen in Mrk 231, a consolidation leftover getting away from its dusty casing.

3 RADIO DATA (Wang et al. 2021)

The nuclear ultra-fast X-ray winds, the ionized gas outflows from the broad-line region, and the galactic-scale molecular and atomic gas outflows are just a few of the powerful multi-phase outflows that Mrk231 is home to (Feruglio et al. 2015; Morganti et al. 2016). In comparison to the X-ray ultra-fast winds (up to 20000 km s^{-1}), the inferred jet flow speed in this work is slightly lower. The inverse correlation between the radio and far-UV luminosity in Mrk 231 indicates a direct connection between the jet and the BAL winds (Reynolds et al. 2017).

The multi-phase multi-scale outflows in active galactic nuclei (AGN) may be enabled by a mixture of driving mechanisms, including the central AGN (radiation pressure), a nuclear starburst (stellar

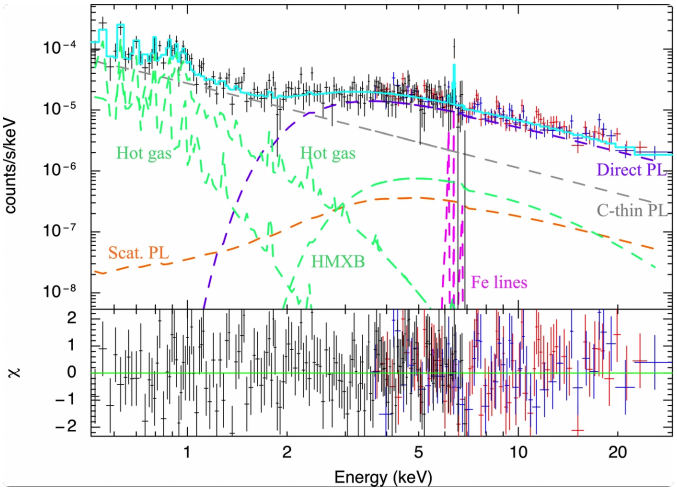

Figure 5. The best-fit model components (dashed lines) are depicted in the unfolded Chandra and NuSTAR spectra, and the overall model is highlighted in cyan. Green is used for the starburst MEKAL and HMXB components. Compton-thin AGN emission that is unaffected by the absorber (gray), "zeroth" order direct AGN emission that is transmitted through the absorber (purple), scattered AGN emission that is transmitted through the absorber (orange), and the Fe K emission lines that are self-consistently modeled within MYTorus in addition to the 6.7 keV Fe line (magenta) are all components of the AGN component.

winds and radiation pressure), and the radio jet (kinetic energy). While the role of AGN-driven winds and outflows (non-relativistic) on feedback at large scales has been investigated in some detail (e.g., Rupke et al. 2017; García-Bernete et al. 2021), the role of the radio jet in driving the outflow in the nuclear region requires clarification (e.g. Morganti et al. 2013). Mrk 231 is one of the few radio-quiet quasars containing a prominent jet. The source shows a triple (core and two lobes) radio morphology structure with an extent of ∼40 pc (50 mas) in the north-south direction, revealed by the European VLBI Network (EVN) observation at 1.6 GHz (Neff & Ulvestad 1988) and the Very Long Baseline Array (VLBA) observations at multiple frequencies from 1.4 to 8.4 GHz (Ulvestad et al. 1999a). The higher-resolution VLBA images at 15 GHz resolve the central component into two compact components separated by ∼1 pc aligning in the northeast-southwest direction (Ulvestad et al. 1999a,b). The northeastern component showed a remarkable variability (Ulvestad et al. 1999b) and was thus identified as the core (the location of the active nucleus). The inner 1-pc position angle of the jet is different from that of the larger 40-pc triple structure by ∼ 60°. Reynolds et al. (2009, 2017, 2020) observed Mrk 231 using the VLBA at higher frequencies of 22 and 43 GHz and obtained a similar core-jet morphology at 1-pc scale. The derived core brightness temperatures, $T_B > 10^{10}$ K, are 2–3 orders of magnitude lower than that of typical blazars (Kovalev et al. 2005), but are consistent with radio-quiet quasars (Blundell et al. 1996; Ulvestad et al. 2005). The kinematic property of the VLBI jet is still under debate. Ulvestad et al. (1999b) determined a jet proper motion speed of $0.14 \pm 0.052\,c$ in the period from 1996.8 to 1998.7, while Reynolds et al. (2017) measured a higher jet apparent speed $> 3.15\,c$ during a flaring state in 2015. This can be explained if Mrk 231 contains episodic fast-moving ($v \approx 1 - 3\,c$) knots and a continuous slower background jet body (Reynolds et al. 2020).

REFERENCES

Aalto S., Garcia-Burillo S., Muller S., Winters J. M., van der Werf P., Henkel C., Costagliola F., Neri R., 2012, A&A, 537, A44
Blundell K. M., Beasley A. J., Lacy M., Garrington S. T., 1996, ApJ, 468, L91
Feruglio C., et al., 2015, A&A, 583, A99
García-Bernete I., et al., 2021, A&A, 645, A21
Kovalev Y. Y., et al., 2005, AJ, 130, 2473
Kramer R. H., Haiman Z., 2009, MNRAS, 400, 1493
Lindberg J. E., et al., 2016, A&A, 587, A15
Morganti R., Fogasy J., Paragi Z., Oosterloo T., Orienti M., 2013, Science, 341, 1082
Morganti R., Veilleux S., Oosterloo T., Teng S. H., Rupke D., 2016, A&A, 593, A30
Neff S. G., Ulvestad J. S., 1988, AJ, 96, 841
Petrov L., Kovalev Y. Y., Fomalont E. B., Gordon D., 2008, AJ, 136, 580
Reynolds C., Punsly B., Kharb P., O'Dea C. P., Wrobel J., 2009, ApJ, 706, 851
Reynolds C., Punsly B., Miniutti G., O'Dea C. P., Hurley-Walker N., 2017, ApJ, 836, 155
Reynolds C., Punsly B., Miniutti G., O'Dea C. P., Hurley-Walker N., 2020, ApJ, 891, 59
Rupke D. S. N., Gültekin K., Veilleux S., 2017, ApJ, 850, 40
Ulvestad J. S., Wrobel J. M., Carilli C. L., 1999a, ApJ, 516, 127
Ulvestad J. S., Wrobel J. M., Roy A. L., Wilson A. S., Falcke H., Krichbaum T. P., 1999b, ApJ, 517, L81
Ulvestad J. S., Antonucci R. R. J., Barvainis R., 2005, ApJ, 621, 123
Veilleux S., Kim D. C., Sanders D. B., 2002, ApJS, 143, 315
Veilleux S., et al., 2006, ApJ, 643, 707
Veilleux S., et al., 2009, ApJS, 182, 628
Veilleux S., et al., 2013, ApJ, 764, 15
Wang A., An T., Jaiswal S., Mohan P., Wang Y., Baan W. A., Zhang Y., Yang X., 2021, MNRAS, 504, 3823

This paper has been typeset from a TEX/LATEX file prepared by the author.

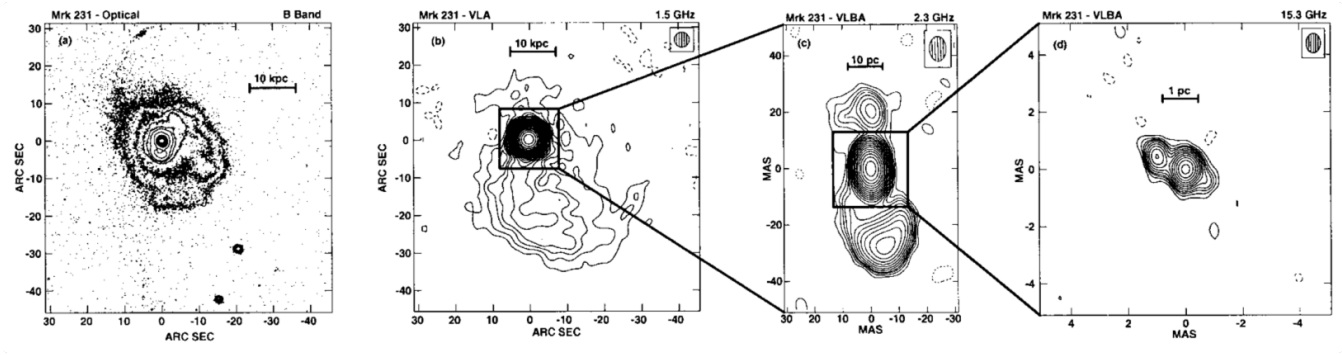

Figure 6. Montage of optical and radio images of Mrk 231. (a) B-band image from Hamilton Keel (1987). (b) VLA 1.5 GHz image, at the same scale as panel a, with the two images aligned according to their respective peaks. (c) Full-resolution VLBA 2.3 GHz image of the core seen in the VLA image. (d) Magnification of full-resolution VLBA 15 GHz image of the central source seen in panel c.

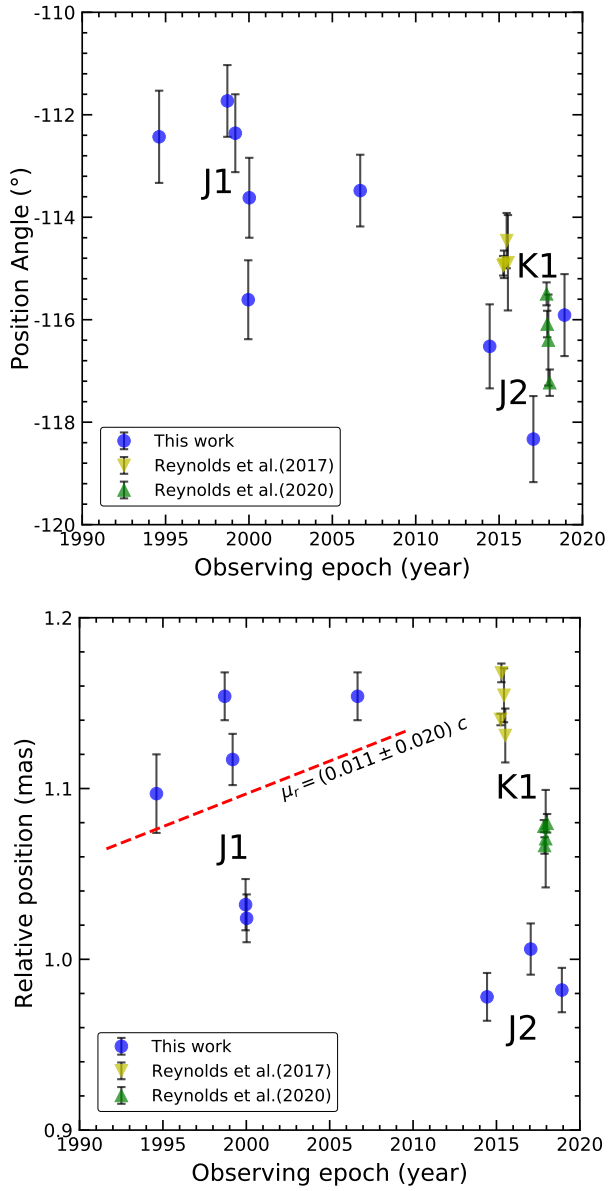

Figure 7. The jet position angle change with time (upper panel) and the relative jet distance with respect to the core versus the observing epoch (bottom panel). Symbols are as follows: blue circles – Astrogeo database (e.g., Petrov et al. 2008), light blue triangles – Ulvestad et al. (1999a), pink hexagon – Reynolds et al. (2017), and green triangle – Reynolds et al. (2020).